CrossMark

RESEARCH ARTICLE

Spray features in the near field of a flow-blurring injector investigated by high-speed visualization and time-resolved PIV

Lulin Jiang[1] · Ajay K. Agrawal[1]

Abstract In a flow-blurring (FB) injector, atomizing air stagnates and bifurcates at the gap upstream of the injector orifice. A small portion of the air penetrates into the liquid supply line to create a turbulent two-phase flow. Pressure drop across the injector orifice causes air bubbles to expand and burst thereby disintegrating the surrounding liquid into a fine spray. In previous studies, we have demonstrated clean and stable combustion of alternative liquid fuels, such as biodiesel, straight vegetable oil and glycerol by using the FB injector without requiring fuel pre-processing or combustor hardware modification. In this study, high-speed visualization and time-resolved particle image velocimetry (PIV) techniques are employed to investigate the FB spray in the near field of the injector to delineate the underlying mechanisms of atomization. Experiments are performed using water as the liquid and air as the atomizing gas for air to liquid mass ratio of 2.0. Flow visualization at the injector exit focused on a field of view with physical dimensions of 2.3 mm × 1.4 mm at spatial resolution of 7.16 μm per pixel, exposure time of 1 μs, and image acquisition rate of 100 k frames per second. Image sequences illustrate mostly fine droplets indicating that the primary breakup by FB atomization likely occurs within the injector itself. A few larger droplets appearing mainly at the injector periphery undergo secondary breakup by Rayleigh–Taylor instabilities. Time-resolved PIV is applied to quantify the droplet dynamics in the injector near field. Plots of instantaneous, mean, and root-mean-square droplet velocities are presented to reveal the secondary breakup process. Results show that the secondary atomization to produce fine and stable spray is complete within a few diameters from the injector exit. These superior characteristics of the FB injector are attractive to achieve clean combustion of different fuels in practical systems.

1 Introduction

Increasing demand for energy, depletion of fossil fuel sources, and consciousness for environmental protection are motivating pursuit of novel approaches to sustainably use both conventional and renewable fuels (Rottenkolber et al. 2002; Dumouchel 2008; Tropea 2011; Sedarsky et al. 2013; Kourmatzis and Masri 2014; Mirsepassi and Rankin 2014). Recently, research in the field of liquid fuel combustion has focused on the utilization of biodiesel and other viscous fuels such as vegetable oils (VOs) and glycerol and on effective methods to atomize such fuels (Szybist et al. 2007; Raghavan et al. 2009; Bohn et al. 2011; Wang et al. 2011; Quispe et al. 2013; Steinmetz et al. 2013). Fine and stable atomization of liquid fuels is directly related to the subsequent clean, efficient, and stable combustion. A fine spray consists of multiple small fuel droplets that can evaporate quickly and mix well with the oxidizer to promote clean premixed combustion, minimizing emissions of soot, carbon monoxide (CO), and nitrogen oxides (NO_x) (Lefebvre 1980; Jiang et al. 2012a, b; Simmons and Agrawal 2012; Jiang and Agrawal 2014a, b). In a conventional twin-fluid atomizer such as air-blast (AB) atomizer, the high-velocity fuel jet is broken down into fine droplets at the shear layer instabilities created by the surrounding flow of the atomizing air (Rayleigh 1883; Taylor 1950; Lefebvre 1980, 1989, 1992). The fineness of the spray in twin-fluid atomizers is affected by several factors such as

✉ Ajay K. Agrawal
aagrawal@eng.ua.edu

1 Department of Mechanical Engineering, The University of Alabama, Box 870276, Tuscaloosa, AL 35487-0276, USA

Springer

the kinematic viscosity and surface tension of the fuel and fuel's interactions with the atomizing air (Lefebvre 1992). In addition, the atomizing air to liquid mass ratio (ALR) is a critical parameter affecting the atomization process (Lefebvre 1992; Simmons and Agrawal 2010). The AB atomization fails to generate fine sprays and clean flames of alternative fuels such as biomass-derived oils that can be up to 10–20 times more viscous than conventional diesel fuel (Panchasara et al. 2009a, b). For example, CO and NO$_x$ emissions from combustion of straight VO atomized by an AB injector were greater than 2000 ppm, exceeding the range of the gas analyzer (Panchasara et al. 2009a, b). Clean combustion of viscous fuels such as VOs using AB injectors requires fuel preheating to reduce the kinematic viscosity and/or heated combustion air supply to provide sufficient heat transfer for rapid droplet vaporization (Bohn et al. 2011; Quispe et al. 2013; Steinmetz et al. 2013).

Effervescent atomization has been investigated to overcome the limitation of conventional injectors for highly viscous liquid fuel applications (Sovani et al. 2001; Linne et al. 2010; Shepard 2011). In an effervescent atomizer, atomizing gas is pressurized into the liquid flow via pores on the mixing chamber wall to form two-phase flow prior to it entering the injector body (Sovani et al. 2001; Gadgil and Raghunandan 2011; Shepard 2011). Gas bubbles expand near the injector exit to break up the surrounding liquid phase into fine spray. However, the internal two-phase flow regime might transition within the injector body from bubbly flow to slug flow with large bubbles or annular flow with merged injected gas surrounded by an annular liquid film. The slug flow regime can produce a pulsating spray resulting from the intermittent flow of large gas voids followed by liquid slugs (Sarkar and Ramamurthi 2007;

Shepard 2011). Recently, Lin et al. (2009, 2011) have designed a new effervescent (or aerated-liquid) injector. For a modest aeration level, it generates a homogeneous-like two-phase flow inside the mixing chamber rather than a bubbly or annular flow (Lin et al. 2009, 2011). Adapters with different configurations are added downstream of the injector exit to further modify the two-phase flow structure (Lin et al. 2014). Measurements in the near field using X-ray radiography indicate that this effervescent injector with adaptors generates highly dispersed sprays (Lin et al. 2014).

A novel concept, called flow-blurring (FB) atomization, has been reported by Gañán-Calvo (2005). FB atomization utilizes the two-phase flow concept similar to effervescent atomization, but it excludes the internal-mixing process within the mixing chamber. In FB atomizers, the two-phase flow forms at the tip of the liquid supply tube. The working principle of the FB atomizer is illustrated in Fig. 1a. As reported by Gañán-Calvo (2005), a portion of the atomizing gas flow enters into the liquid supply tube through the gap between the tube tip and the injector orifice to form a two-phase flow. For liquid supply tube inside diameter, D, equal to the injector orifice diameter, the airflow bifurcates and a two-phase flow is created in the liquid line if the gap between the liquid tube tip and the injector orifice, H, is less than or equal to $0.25D$. Agrawal et al. (2013) designed a transparent injector to observe the internal flow structure illuminated by a warm white LED light and imaged using a high-speed camera (MotionPro HS-4) with exposure time of 31 μs and spatial resolution of 20 μm. The internal flow visualization has revealed the key features including the penetration of the atomizing gas into the liquid supply line, and
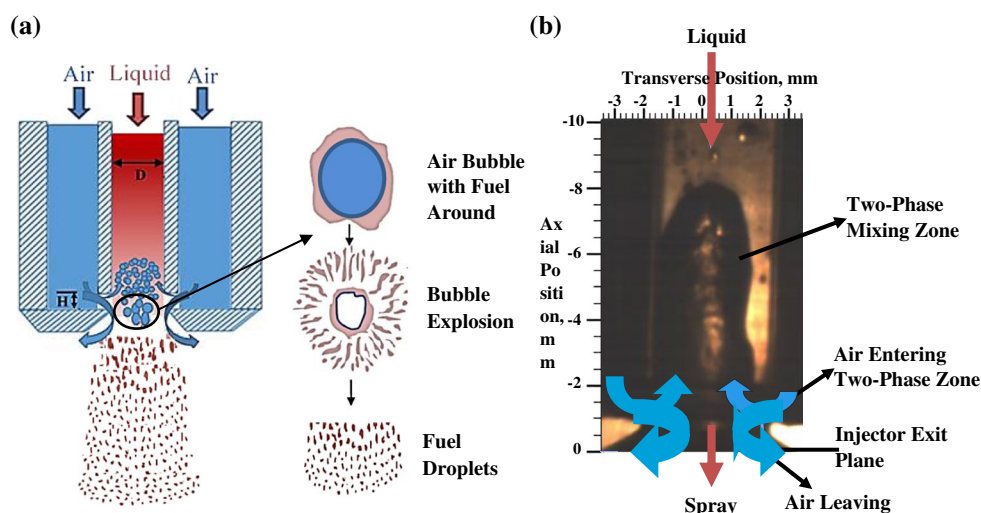

Fig. 1 **a** Working principle of the flow-blurring injector and **b** the internal visualization of a FB injector (Agrawal et al. 2013)

the formation of the turbulent bubble generation zone at the tip of the liquid supply line as shown by the image in Fig. 1b (Agrawal et al. 2013). The two-phase flow exits through the injector orifice where a sudden pressure drop causes gas bubbles to expand and burst. The surrounding liquid is therefore broken into fine droplets during the bubble bursting (Gañán-Calvo 2005). FB injector produces stable and fine spray without the need for very high pressure atomizing gas as demonstrated in our previous studies without and with combustion (Panchasara et al. 2009a, b; Simmons et al. 2009; Simmons and Agrawal 2010, 2012; Simmons 2011; Jiang et al. 2012a, b; Jiang and Agrawal 2014a, b).

Figure 2 visually illustrates significant qualitative differences in water sprays formed by AB and FB injectors for identical water and air flow rates with ALR = 3.5. These images represent a field of view (FOV) of 7 mm × 7 mm immediately downstream of the injector exit to highlight the key features of the spray. Note that different exposure times were necessary to acquire observable images for the two cases; FB injector produced smaller droplets which required longer exposure time to yield sufficient scattered light for visual imaging. Figure 2 reveals that the AB injector produces the typical liquid core in the near field, while for the same liquid and gas flow rates, the FB injector forms fine spray, illustrating the significantly improved atomization capability of the latter. Phase Doppler particle analyzer (PDPA) measurements have also shown that for given liquid and atomizing air flow rates, the FB injector produces finer spray than the AB injector (Simmons et al. 2009; Simmons 2011). Radial profiles of droplet diameter distribution in the water spray with the FB injector showed Sauter mean diameter (SMD) ranging from 7 to 25 μm and the largest droplet diameter of about 30 μm. However, the

AB injector produced SMD in the range of 7–45 μm and the largest water droplet diameter of about 80 μm. PDPA measurements in cold sprays of diesel, viscous VO and reacting glycerol spray quantitatively showed that the FB injector produces fine sprays for all of these fuels with flow-weighted average SMD of about 30–40 μm measured, respectively, at axial locations of 2–10 cm downstream of the injector exit (Simmons 2011).

In addition, previous combustion studies by our research group have shown that the FB injector results in cleaner combustion of conventional fuels such as kerosene and diesel. FB injectors decreased CO and NOx emissions in kerosene and diesel flames by 3–5 times compared to those from AB injectors (Panchasara et al. 2009a, b). With the FB injector, biodiesel, straight VO, and glycerol were combusted, in the same system, stably and cleanly with ultra-low emissions of CO and NO_x, overcoming the limitation of the current AB atomizers (Simmons 2011; Jiang et al. 2012a, b; Simmons and Agrawal 2012; Jiang and Agrawal 2014a, b).

In prior studies, measurements of droplet diameter and velocity in the spray were acquired by the PDPA technique, at locations at least 1.0 cm downstream of the injector exit. Droplet diameter distributions presented in these studies show excellent atomization capability of the FB injector for liquids with wide range of viscosities including water, diesel, VO, and glycerol (Simmons et al. 2009; Simmons and Agrawal 2010; Simmons 2011). However, no measurements have so far been acquired in the injector near field, which is important to understand the details of the liquid breakup processes (e.g., bubble bursting) and eventually to relate the spray properties to the FB injector geometry and operating conditions. In an AB injector, the near-field measurements are difficult to acquire by PDPA and other quantitative techniques because of the presence of a

Fig. 2 Water sprays at liquid flow rate of 8 ml/min and ALR = 3.5 for **a** an AB injector with spatial resolution of 20 μm and exposure time of 1 ms and **b** a FB injector with spatial resolution of 33 μm and exposure time of 10 ms
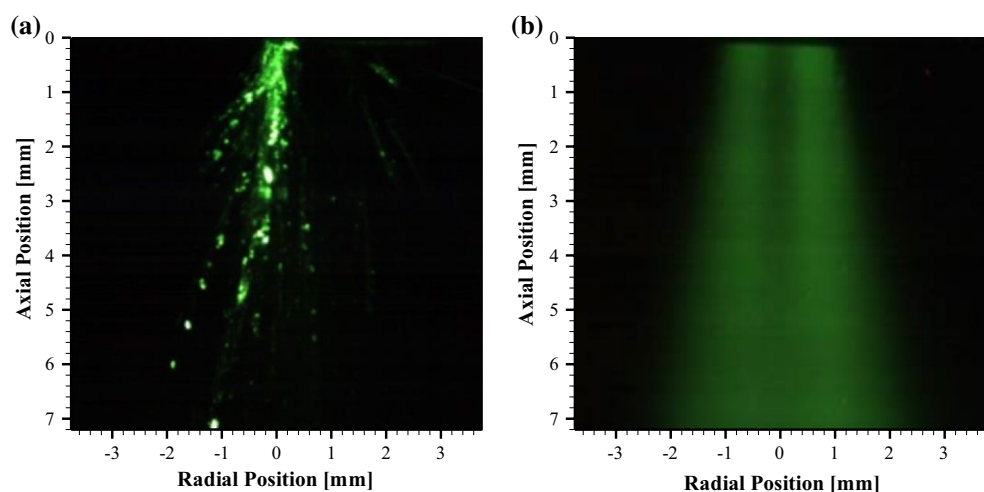
dominant liquid core (see Fig. 2a). However, a fine spray from the FB injector (e.g., Fig. 2b) offers the opportunity to employ advanced flow diagnostics techniques to understand the liquid breakup process in the near field. Thus, this study seeks to characterize the near field of the FB injector using high-speed imaging and time-resolved particle image velocimetry (PIV). The primary objective is to gain insight into the FB spray features including droplet dynamics and droplet breakup processes. PIV is used to measure the droplet velocity rather than the gas phase velocity, which is expected to be higher.

2 Experimental setup

2.1 Flow-blurring injection system setup

The schematic of the in-house built FB injector setup producing spray at the ambient conditions is shown in Fig. 3. The inside diameter, D, of the liquid supply tube as well as that of the injector orifice is 1.5 mm. The gap between the liquid supply tube tip and injector orifice, $H = 0.375$ mm, is used to fulfill the requirement for FB atomization. Water, chosen as the working liquid, is pumped by a Cole Parmer high performance peristaltic metering pump (Model 7523-40) with an accuracy of ± 0.25 % of the reading. A four-roller pump head (Masterflex L/S Easy-Load II Head), a pulsation dampener, and a long soft discharge tube are used to eliminate any pulsations to ensure a steady supply of the water flow. Water enters the injector holder from the side before flowing into the injector connected with the holder. Atomizing air (AA) is supplied from the upstream of the injector holder at a pre-set flow rate measured by an Aalborg mass flow meter (Model CFM47) with an accuracy of ± 1.5 % of the reading. Air flow rate of 20 standard liters per minute (slpm) and water flow rate of 12 ml/min are utilized to obtain an ALR = 2.

2.2 High-speed visualization setup

A high-speed camera (Photron FASTCAM SA5) mounted with 100-mm focal-length lens, a 2× extender and 130 mm length of extension tubes is used to acquire visual images for a small FOV with dimensions of 2.3 mm × 1.4 mm at the injector exit. For acquisition rate of 100,000 fps, the image renders spatial resolution of 7.16 μm per pixel, to distinguish individual, though, stationary droplets; all spatial resolutions listed in this study refers to actual (measurable) spatial resolutions. Background illumination is provided by a very high intensity white light source (Energetiq LDLS) produced by a laser-driven plasma to minimize the blurring caused by the droplet motion during the camera exposure time of 1 μs; still a droplet at a velocity of 100 m/s will move about 100 μm during the camera exposure time. Thus, only slow-moving, larger droplets can be accurately detected in practice. Note that a calibration target is utilized to focus the camera on the center plane of the spray in an attempt to distinguish droplets at the center from those away from the center.

2.3 Particle image velocimetry (PIV) setup

The time-resolved PIV technique was used to measure the droplet velocity in the injector near field. As shown in the schematic diagram in Fig. 3, a dual head Nd:YAG laser (Quantronix Hawk-Duo 532-12-M laser with the wave length of 532 nm and average power of 120 W) is used to produce two laser pulses with time interval of 1 μs at repetition rate of 15 kHz. TSI divergent sheet optics with −15 mm focal-length cylindrical lens and 1000-mm spherical lens is used to form a 1-mm-thick laser sheet to illuminate the FOV. A high-speed camera (Photron FAST-CAM *SA5*) with a microscopic lens set perpendicularly focuses on the laser sheet with the total viewed area of 8.6 mm × 8.6 mm, yielding spatial resolution of 16.83 μm per pixel. The camera is synchronized with the time setting

Fig. 3 Schematic of **a** the injection system and PIV experimental setup, and **b** flow paths in the FB injector
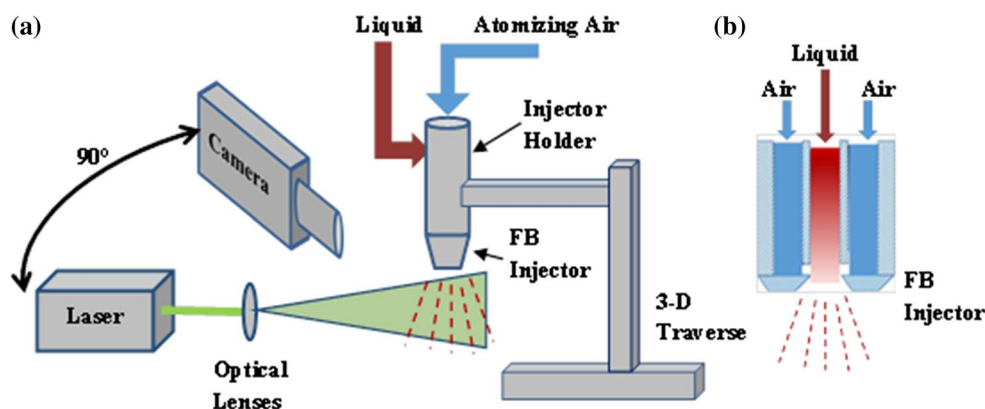
of the laser pulses to acquire image pairs at an interval of 1 μs and image pair acquisition rate of 15 kHz.

Frame-straddled images are analyzed using Insight software (version 4.0 TSI Inc) with the cross-correlated subregions of image pairs to generate the velocity vectors of the near-field FB spray. The initial interrogation window size of 64 × 64 pixels with 50 % overlap spacing is used to calculate the velocity vectors. This small window size minimizes the particle-correlation noise and still includes more than ten effective particle pairs, ensuring nearly 100 % valid velocity measurements (Keane and Adrian 1992). For the present setup, the ratio of out-of-plane displacement to the light sheet thickness (1.0 mm) is about 0.005, much less than the maximum acceptable level of 0.25 required by the analyzing software. Thus, the out-of-plane motion has a negligible effect on the accuracy of the velocity measurements. Spurious vectors are eliminated using three methods. First, a local median test is applied to filter out the vectors. When the difference between the current velocity vector and the local median velocity of neighboring vectors exceeds the given tolerance (two times of the local median value), the vector is rejected and replaced by a valid secondary peak. Second, a vector is valid when the signal to noise ratio is >1.4. A range filter is applied to reject the vectors exceeding reasonable limits in the axial (V) and radial (U) displacements. The holes in the vector field are filled using a recursive filling procedure employing the local mean. It first fills the holes with the most valid neighbors and then the ones with second most valid neighboring vectors.

3 Results and discussion

3.1 Spray visualization

3.1.1 Primary breakup by FB atomization

Figure 4 shows consecutive high-speed images of a FB spray in the near field of the injector. As explained above, the images are acquired at spatial resolution of 7.16 μm per pixel, exposure time of 1 μs, and frame speed of 100 kHz. In contrast to the large FOV and long-exposure (33 ms) image of the FB spray in Fig. 2b, the small FOV and short exposure time for the images of Fig. 4 make it experimentally feasible to visualize the instantaneous spray structure in detail. Figure 4 depicts an occasionally observed air bubble at the injector exit that expands, bursts, and disintegrates the surrounding liquid into droplets, visually illustrating the liquid breakup by FB atomization. These air bubbles at the spray center were detected irregularly, once every 10,000 images or at time interval of about 100 ms. Interestingly, the majority of the liquid exited the injector already atomized into
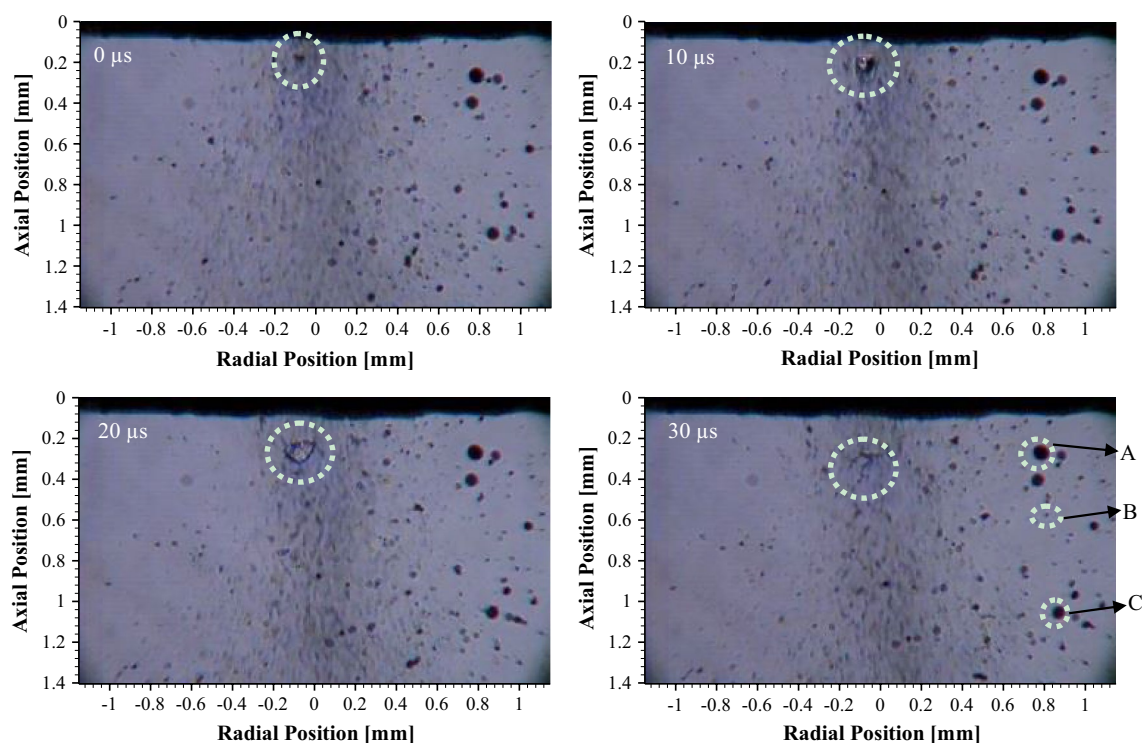

Fig. 4 Spray visualization in the injector near field for ALR = 2.0 at spatial resolution of 7.16 μm/pixel and exposure time of 1 μs

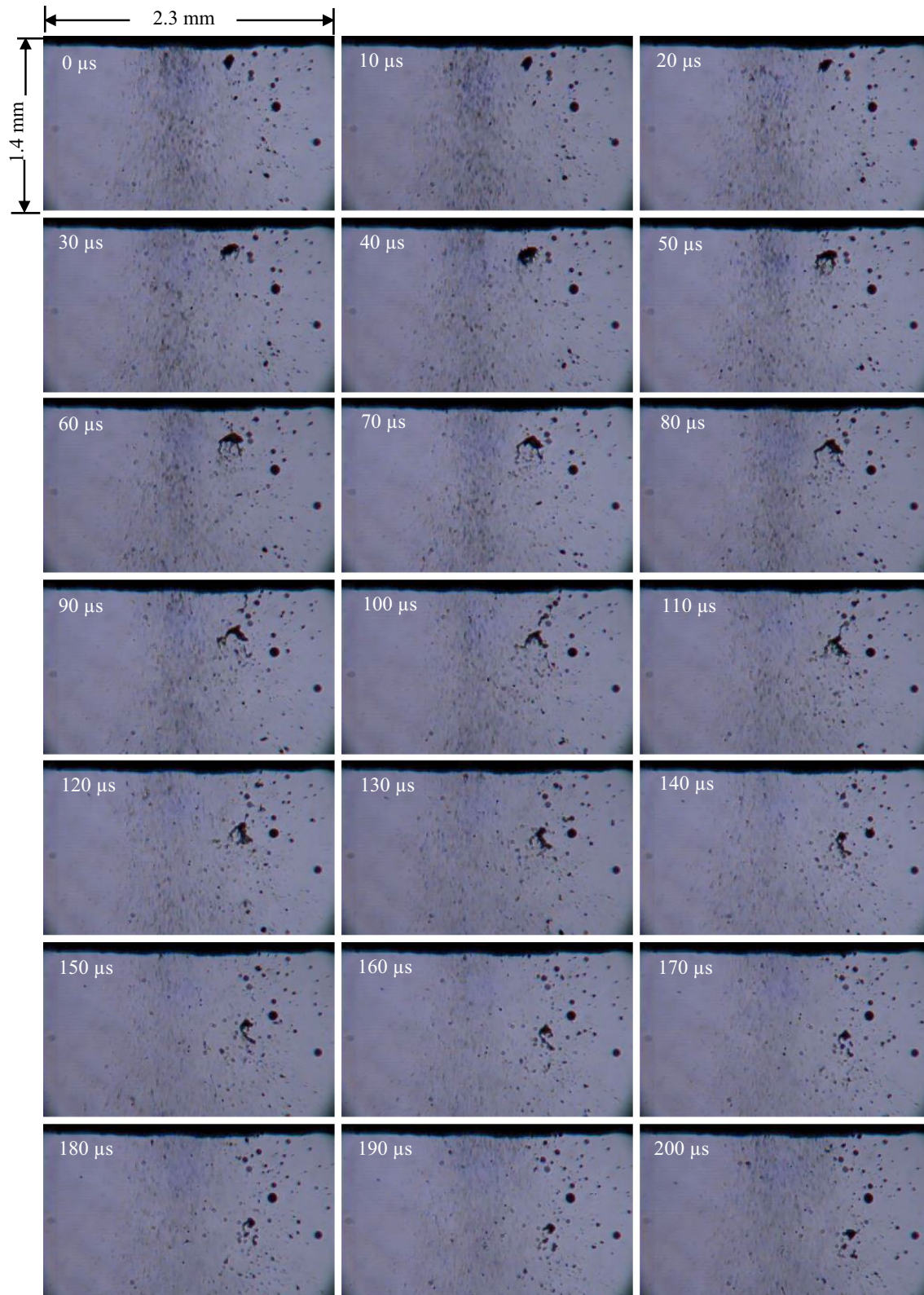**Fig. 5** FB droplet breakup in the injector near field captured at spatial resolution of 7.16 μm/pixel, exposure time of 1 μs and frame speed of 100 kHz. ALR = 2.0

fine droplets, except for some larger droplets at the spray periphery as shown in Fig. 4. These results show that the liquid breakup by bubble bursting or FB atomization likely occurs mainly upstream of the injector exit and possibly within the discharge orifice. Bubble bursting is hereby denoted as the primary breakup by the FB atomization. Note that the FB atomization within the injector is not optically accessible in this experiment because of the instrumentation and hardware limitations.

Most of the droplets generated by primary breakup cannot be spatially resolved in the images because of the blurring caused by the droplet motion in spite of the camera exposure time of 1 μs. However, larger droplets on the injector periphery are spatially and temporarily resolved. Note that the asymmetry in the images is the result of minor geometric imperfections of the in-house built FB injector. In Fig. 4, the diameter of droplet A is about 100 μm, of droplet B is about 21 μm and that of droplet C is about 72 μm.

3.1.2 Secondary breakup by Rayleigh–Taylor instabilities

Figure 5 shows consecutive images for 200 μs to illustrate the secondary breakup of the larger droplets in the injector near field. The larger droplets are observed mainly away from the spray center and are concentrated mostly near the periphery of the injector orifice, i.e., in the shear layer region. These larger droplets gradually deform by Rayleigh–Taylor instabilities between the liquid and the fast-moving atomizing air flow and breakup into smaller droplets within a short distance from the injector exit. This external atomization of larger droplets is denoted as the secondary breakup by Rayleigh–Taylor instabilities. While larger droplets always appeared at the spray periphery, they also appeared occasionally at the spray center close to the injector exit at time intervals of 0.92 to about 2.30 ms (not shown here for brevity, but also verified by PIV images). Again, these droplets quickly broke-up into smaller droplets by secondary atomization as discussed above.

In order to characterize the secondary breakup, Weber (We) number and Ohnesorge (Oh) number are quantitatively estimated for the present flow conditions (Weber 1931; Ohnesorge 1936; Faeth 2002; Batarseh 2008). Weber number represents the ratio of the kinetic force because of the relative motion (at U_r) between droplets and atomizing air and the surface tension. Ohnesorge number indicates the ratio of the viscous force to the surface tension. In the present study, the atomizing air velocity is about 120 m/s and the relative velocity is estimated to vary from 20 to 100 m/s (confirmed by PIV measurements). Figure 6a shows that the Weber number in the near field is <15. Figure 6b illustrates that the Ohnesorge number decreases as the droplet diameter increases, indicating that the viscous force is more easily overcome in larger droplets to help with the secondary atomization.

In summary, the spray visualization experiments show that most of the liquid is atomized by bubble bursting likely within the FB injector to produce fast-moving, fine droplets in the center region of the spray. Slow-moving, larger droplets with diameter ranging from 20 to 100 μm are observed occasionally at the center, but mainly at the periphery close to the injector exit. These larger droplets quickly disintegrate into smaller droplets because of secondary atomization by the Rayleigh–Taylor instabilities. The secondary atomization would be even more effective in practical systems where, in addition to the atomizing air, the droplets can also interact with the combustion air.
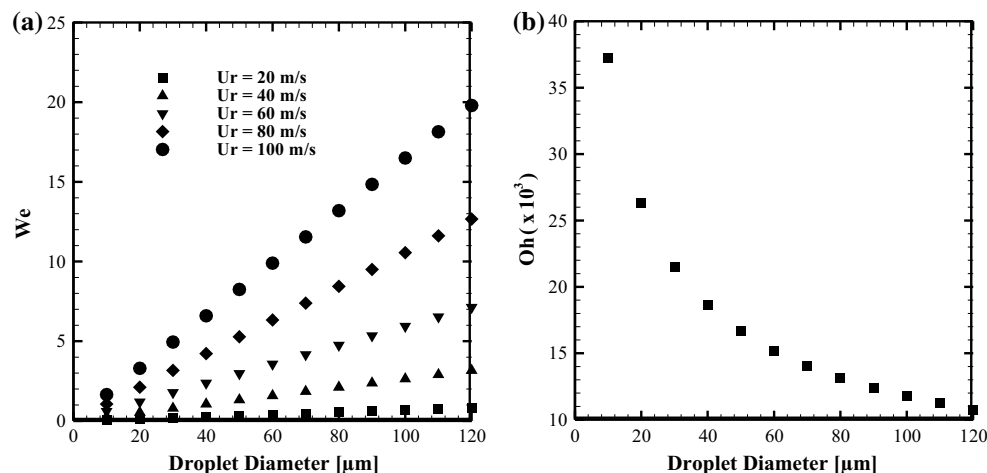

Fig. 6 Weber (We) number and Ohnesorge (Oh) number for water spray in the FB injector near field

3.2 PIV measurements

The spray visualization results clearly revealed the atomization process in the FB injector and preliminarily reflected the inverse relationship between the droplet diameter and the droplet velocity. Finer droplets move faster, while larger droplets travel slower. PIV is utilized to measure the droplet velocity and to quantitatively explore the spray dynamics in the near field of the FB injector. The measurements are obtained by positioning the laser sheet and camera focus at a plane across the center of the spray. The analysis is based on 1500 frame-straddled image pairs.

3.2.1 Instantaneous droplet dynamics

Figure 7a, b shows a PIV image pair at time interval of 1 μs. The images pertain to FOV of 7.6 mm × 7.6 mm, frame speed of 30 kHz (15 k image pairs per second), and spatial resolution of 16.83 μm per pixel. The high laser intensity and image exposure time of <150 ns determined by the laser pulse duration essentially freezes the fast-moving droplets which could not be spatially and temporally resolved at the camera exposure time of 1 μs in the flow visualization experiment discussed above. PIV images also reveal that the FB spray contains mainly fine droplets in the near field. Similar to the previous results, some larger droplets indicated by brighter spots also appear near the injector periphery. These larger droplets interact with the atomizing air and breakup into smaller droplets at downstream locations as discussed above. Overall, PIV images vividly illustrate the FB injectors' capability of generating fine droplets in the near field. PIV image pair in Fig. 7a, b is used to compute the instantaneous droplet velocity field shown in Fig. 7c. Results show that the droplet velocity increases in the flow direction signifying that the slower-moving, larger droplets at the injector exit are accelerated by the gas phase to produce smaller droplets by the secondary atomization. The atomized fine droplets at downstream locations travel faster as they tend to follow the high-velocity atomizing air flow.

Next, the temporal behavior of instantaneous droplet axial velocity at the center and periphery of the spray is explored in Fig. 8 at four different axial planes; near the injector exit ($y = 0.50$ mm), farther downstream or at the end of the PIV FOV ($y = 6.50$ mm), and in between ($y = 2.00$ and 3.50 mm). Measurements are shown for time span of 50 ms representing a set of 750 data points, feasible because of the time-resolved feature of the PIV system. Closest to the injector ($y = 0.50$ mm), majority of the droplets at the spray center ($x = 0.00$ mm) travel in the velocity range of 60–80 m/s, while few larger droplets with axial velocity of 20 m/s or even smaller are also observed. Axial velocity of 20 m/s or less signifies occasional slow-moving,
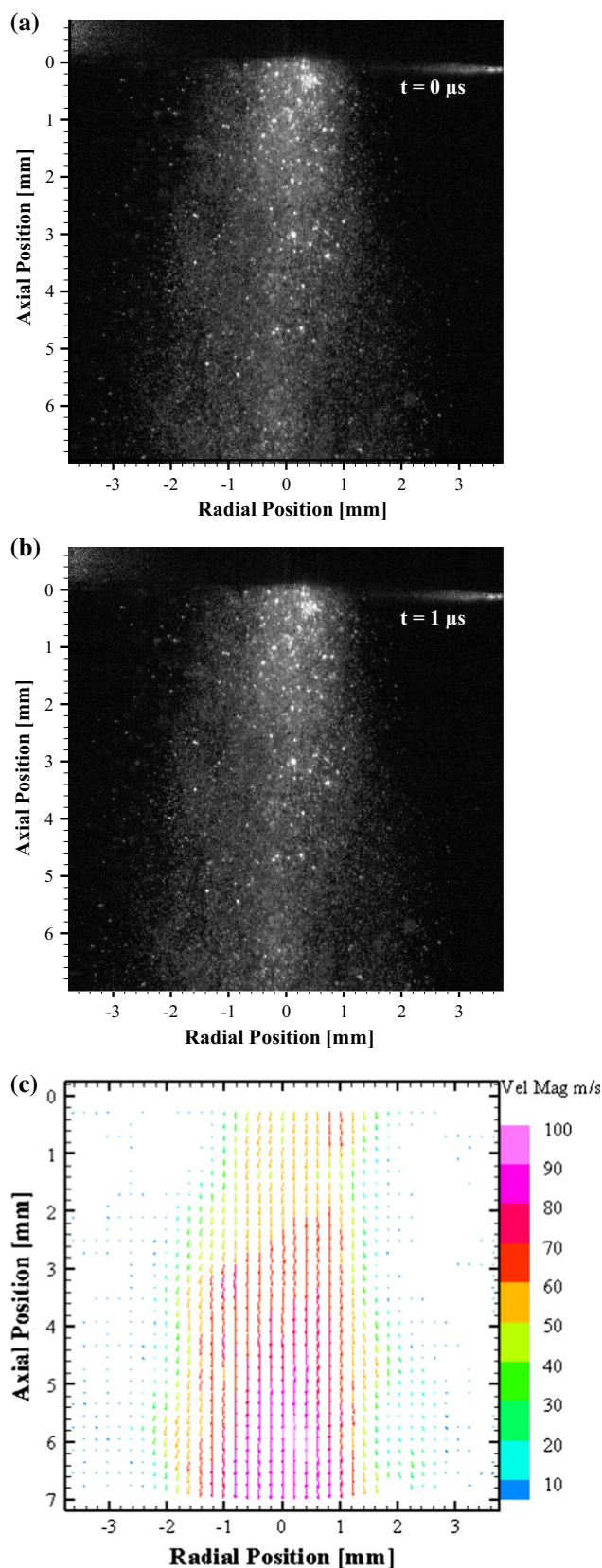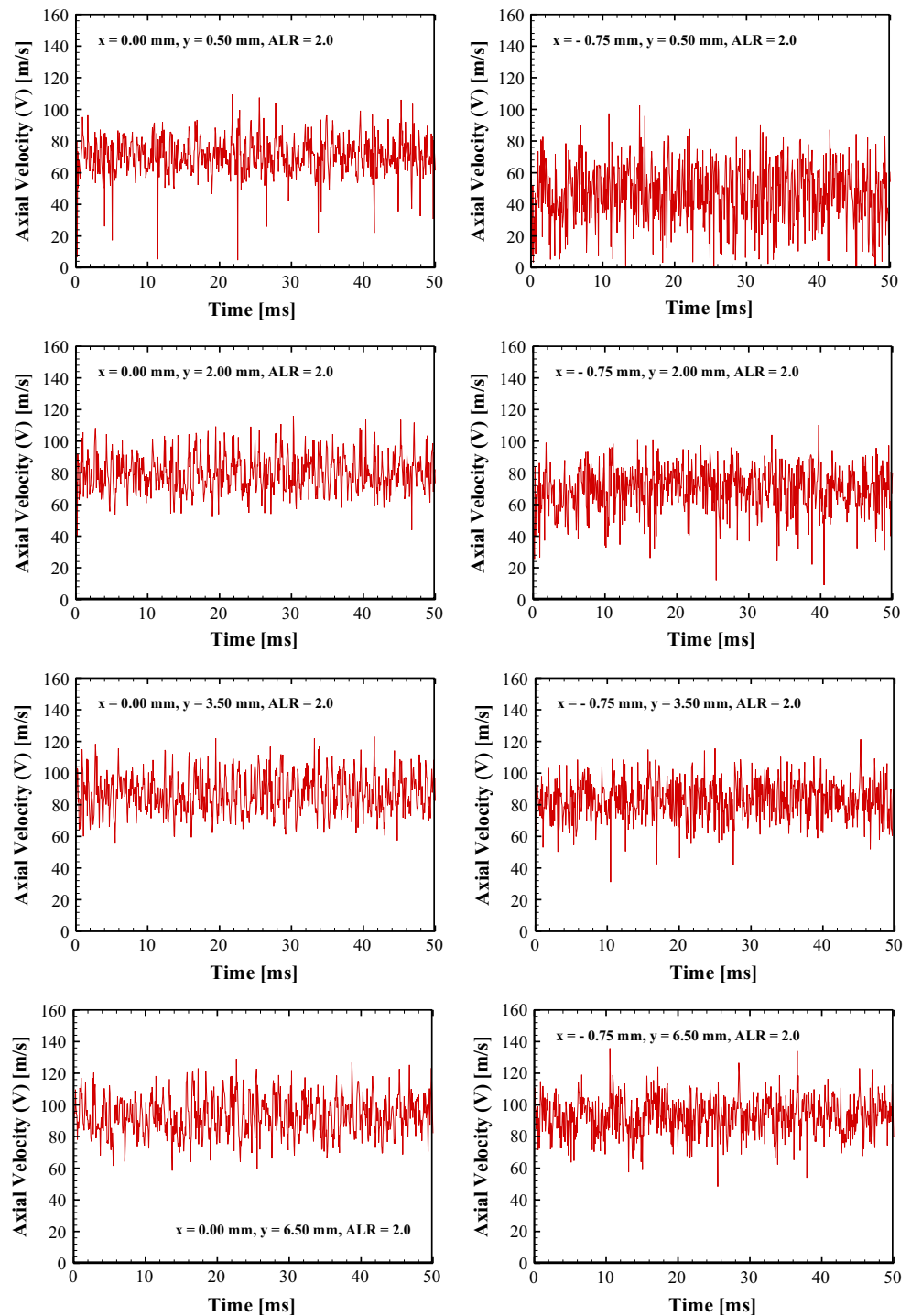

Fig. 7 A FB spray image pair of **a** and **b** captured at 15 kHz and 16.83 μm/pixel, and **c** the computed instantaneous droplet velocity field. ALR = 2.0

Fig. 8 Time analysis of instantaneous axial velocity at the spray center and periphery at different axial locations for ALR = 2.0

larger droplets or air bubbles. These results are consistent with the images in Fig. 4 and indicate that the most of liquid in the center region has been atomized into fast-moving, fine droplets by primary FB atomization. At the spray periphery ($x = -0.75$ mm), the axial velocity varies between 20 and 60 m/s with more frequent occurrences of 10 m/s or even smaller. Again, these results signify a greater number of larger droplets at the spray periphery,

which agrees with the spray visualizations in Figs. 4 and 5. Since FB atomization is nearly complete at the injector exit, the bubble bursting process is likely occurring upstream, i.e., at the injector orifice. The short distance and hence small residence time between formation and bursting of bubbles in the FB injector prevents the two-phase flow to transition among different regimes, thereby resulting in a stable spray.

Fig. 9 Probability of axial velocities at radial location of **a** ▶ $x = 0.00$ mm, **b** $x = -0.20$ mm and **c** $x = -0.75$ mm within 0.1 s

At the downstream location of $y = 2.00$ mm, the droplet velocity range shifts to higher values of 60–100 m/s in the spray center and 40–90 m/s at the spray periphery. At this location, low velocity (say <30 m/s) is absent at the center and occurs less frequently at the periphery. These quantitative results signify secondary atomization between $y = 0.50$ and 2.00 mm, presumably by the Rayleigh–Taylor instabilities. The secondary atomization has disintegrated nearly all of the larger droplets at the spray center and a majority of such droplets at the spray periphery. Droplet acceleration and disintegration by secondary atomization is still evident between $y = 2.00$ and 3.50 mm, despite at a slower pace. The change in droplet velocity between $y = 3.50$ and 6.50 mm is negligible, indicating that the secondary atomization is complete within a short axial distance of about 5.00 mm (3.3D) from the injector exit. Random fluctuations in droplet axial velocity in Fig. 8 are attributed to the turbulent nature of the atomizing air flow, which has the estimated Reynolds number of 1.16×10^4 at the injector exit.

3.2.2 Statistics of droplet dynamics

Next, a total of 1500 data acquired over the 100 ms are used to delineate the statistical features of the droplets in the injector near region. Figure 9 shows the probability of the axial velocity at several locations to quantify the droplet movement in the near field. Results are presented for three transverse locations ($x = 0.00$, -0.20, and -0.75 mm), and for each case, profiles are shown near the injector exit ($y = 0.50$ mm), toward the end of the FOV ($y = 6.50$ mm), and at an in-between location ($y = 3.50$ mm). At the injector exit, majority of the droplets in the center region ($x = 0.00$ and -0.20 mm) have an axial velocity of about 75 m/s, which corresponds to finer droplets that follow the high-velocity atomizing airflow. Droplet acceleration in the core region between $y = 0.50$ and 3.5 mm is clearly evident from Fig. 9a, b, which show peak droplet velocity of about 100 m/s at $y = 3.5$ mm. Droplet acceleration still occurs between $y = 3.50$ and 6.50 mm, although the change in probability curves between these two locations is less significant. Probability curve at the spray periphery ($x = -0.75$ mm) shows a much smaller peak velocity of about 60 m/s at the injector exit, followed by rapid acceleration to peak velocity of about 95 m/s at $y = 3.50$ mm and to 110 m/s at $y = 6.50$ mm. In fact, at the end of the FOV, i.e., $y = 6.50$ mm, the profiles of probability of axial velocity at the three transverse locations nearly overlap with
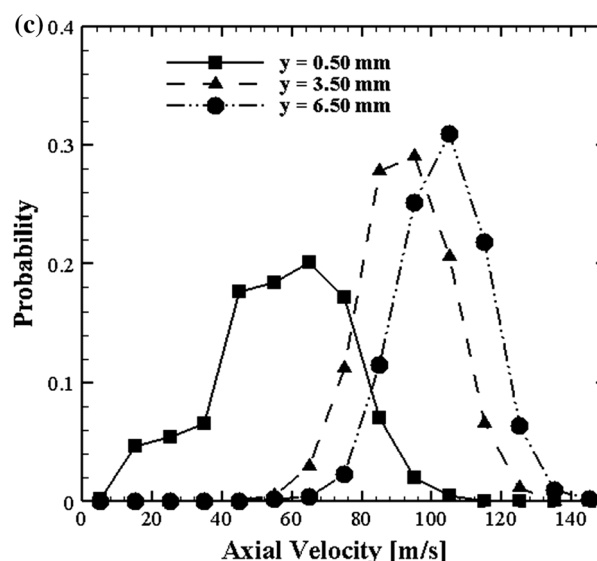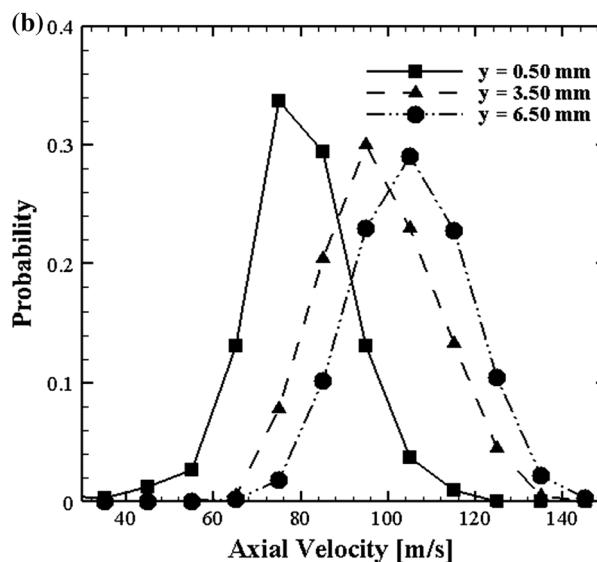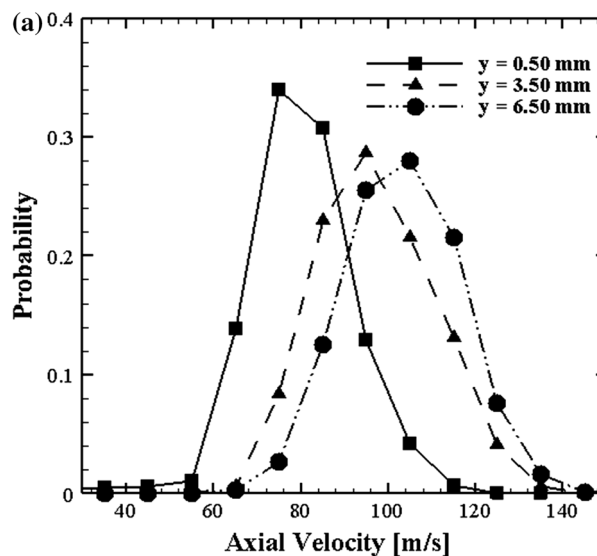
each other further confirming that the secondary atomization has completed at this axial location.

Figure 10a shows that the time-averaged droplet velocity increases in the flow direction and decreases from the center to the periphery of the spray. Again, this result is consistent with the spray visualization results showing some slower-moving, larger droplets mainly at the injector periphery that disintegrate into smaller, faster-moving droplets by secondary atomization at downstream locations. The average axial and radial velocity contours, respectively, in Fig. 10b, c offer quantitative details of the droplet dynamics. At any axial plane, the axial velocity is the highest at the center and it decreases in the radial direction. As expected, the radial extent of the spray increases in the flow direction. Figure 10c illustrates that the droplet radial velocity is generally an order of magnitude smaller than the droplet axial velocity. In Fig. 10, the droplet velocity increases in the flow direction until about $y = 5.00$ mm, indicating that the secondary atomization is nearly complete at this axial location.

Radial profiles of droplet axial and radial velocities at various axial planes in Fig. 11a, b provide quantitative insight into the evolution of the spray in the near field. At the center of spray, the average axial velocity ranges between 70 and 100 m/s, while away from the center, at $x = 1.00$ mm, this range widens to 30 and 80 m/s. This result illustrates that in comparison with the spray periphery, a greater number of faster-moving smaller droplets are present at the spray center, which is consistent with the radial profiles of the SMD measured by Simmons and Agrawal (2010) using the PDPA technique. The average droplet radial velocity is the highest in the shear layer region around $x = 1.00$ mm. The nearly overlapped profiles of both axial and radial velocities at farther downstream locations ($y > 5.00$ mm) signify that the droplet breakup process by secondary atomization is complete within a short distance of the injector exit.

Next, contour plots of root-mean-square (RMS) axial and radial velocities are presented in Fig. 12 to further illustrate the droplet statistics. Figure 12a shows that the RMS droplet axial velocity is the highest at the spray periphery where large but slow-moving droplets appear and disintegrate into finer fast-moving droplets. Moreover, the greatest fluctuations in the axial velocity occur at the injector exit where primary breakup by FB atomization is nearly complete. Figure 12b shows that the RMS radial velocity is higher at the spray periphery, especially at the injector exit. RMS droplet axial and radial velocities are nearly independent of the axial location for $y > 5.00$ mm, again signifying that the secondary atomization by Rayleigh–Taylor instabilities is complete within a short axial distance of about 5 mm or 3.3D.
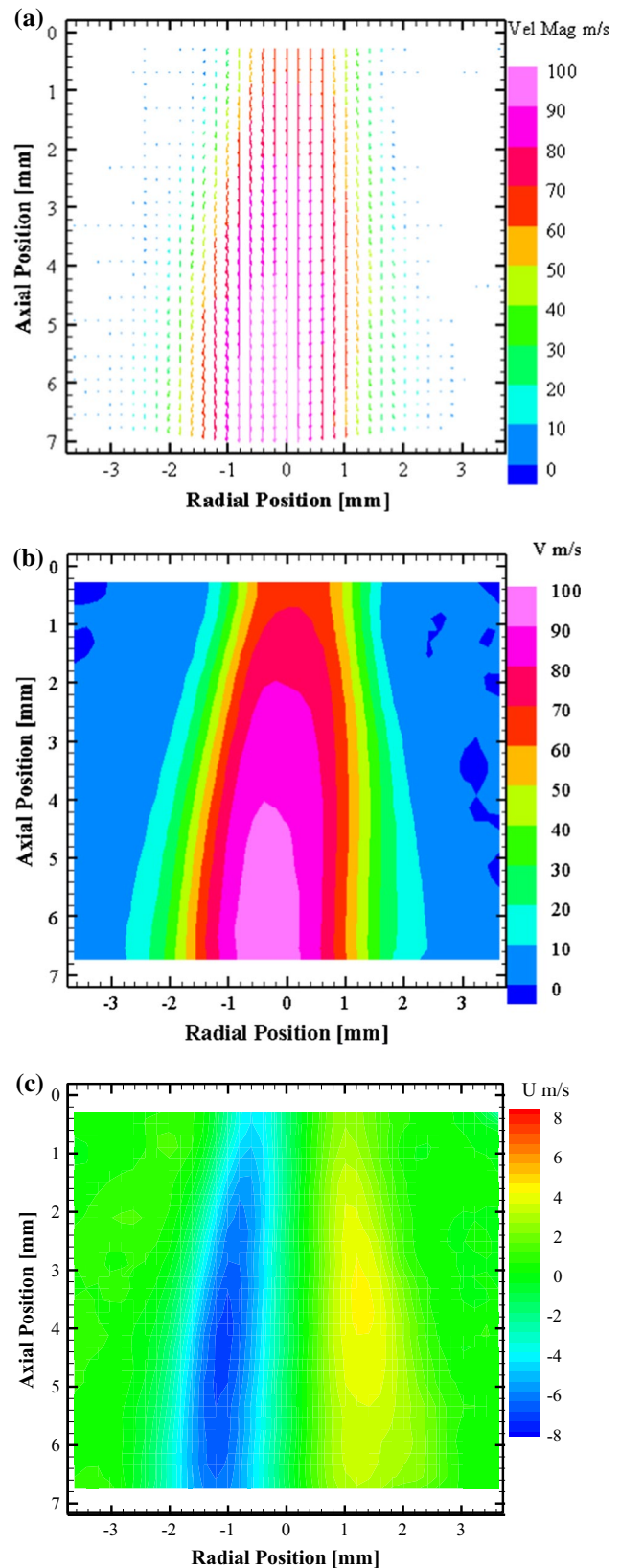
Fig. 10 Time-averaged field: **a** velocity vectors, **b** axial velocity contour and **c** radial velocity contour

Fig. 11 Profiles of time-averaged **a** droplet axial velocity and **b** droplet radial velocity
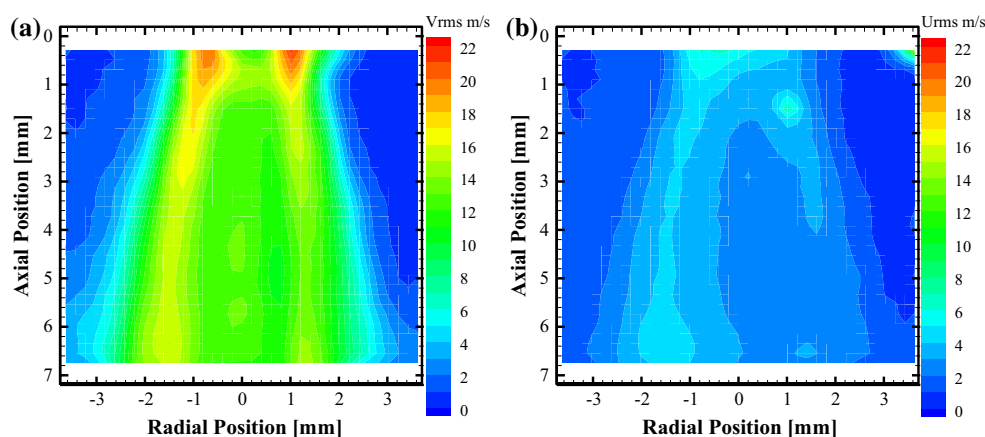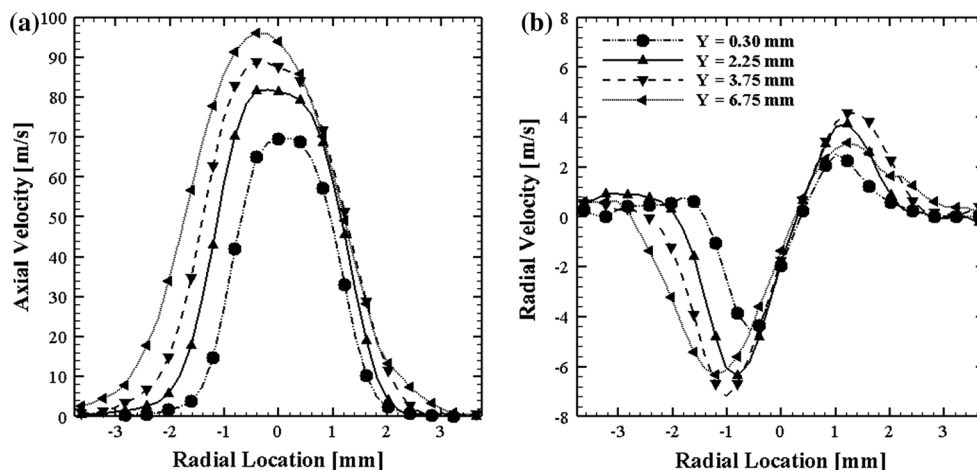

Fig. 12 Contours of **a** RMS droplet axial velocity and **b** RMS droplet radial velocity

4 Conclusions

Detailed dynamic features in the near field of FB injector using water are visualized by high-speed imaging and quantitatively characterized using time-resolved PIV. The atomization process consists of the primary breakup by bubble bursting or FB atomization and the secondary breakup by the typical Rayleigh–Taylor instabilities between the liquid and high-velocity atomizing air. Spray images show that most of the liquid exiting the injector has already been atomized into fine droplets, indicating that the bubble bursting likely takes place mainly within the injector. Few larger droplets with diameter ranging from around 20 to 100 μm appear in the shear layer region at the injector exit and occasionally at the spray center. These larger droplets quickly disintegrate into smaller droplets by the secondary atomization.

PIV measurements are consistent with the flow visualization results and reveal the inverse relationship between the droplet diameter and droplet velocity. Fine droplets follow the high-velocity atomizing air and move faster, while larger droplets travel at slower speed. Temporal analysis of droplet axial velocity reveals how droplets in the center and outer regions accelerate near the injector exit and quickly reach the same velocity range within axial distance of 5.0 mm (or 3.3*D*) where secondary atomization in nearly complete. Probability profiles of axial velocity further confirm these results. The time-averaged velocity field shows that the droplet velocity increases in the flow direction and decreases from the center to the periphery of the spray. This trend is associated with the diameter of the droplets in different regions of the spray as revealed from flow visualization experiments. RMS axial and radial velocities show the greatest fluctuations at the spray periphery of the injector exit.

References

Agrawal SR, Jiang L, Agrawal AK, Midkiff KC (2013) Analysis of two-phase flow inside a transparent fuel injector. In the 8th U. S. National Combustion Meeting of the Combustion Institute, Salt Lake City, UT, USA, Paper no. 070HE-0317

Batarseh FZM (2008) Spray generated by an airblast atomizer: atomization, propagation and aerodynamic instability. Dissertation, TU Darmstadt, Germany

Bohn MD, Metzger BA, Linak WP, King CJ, Roberts WL (2011) Glycerol combustion and emissions. Proc Combust Inst 33(2):2717–2724

Dumouchel C (2008) On the experimental investigation of primary atomization of liquid streams. Exp Fluids 45:371–422

Faeth GM (2002) Dynamics of secondary drop breakup—a rate controlling process in dense sprays. In: Proceedings ILASS-Europe. Invited lecture

Gadgil HP, Raghunandan BN (2011) Some features of spray breakup in effervescent atomizers. Exp Fluids 50:329–338

Gañán-Calvo AM (2005) Enhanced liquid atomization: from flow-focusing to flow-blurring. Appl Phys Lett 86(21):2141–2142

Jiang L, Agrawal AK (2014a) Clean combustion of different liquid fuels using a novel injector. Exp Therm Fluid Sci 57:275–284

Jiang L, Agrawal AK (2014b) Combustion of Straight glycerol with/without methane using a fuel-flexible, low-emissions burner. Fuel 136:177–184

Jiang L, Kolhe PS, Taylor, RP, Agrawal AK (2012a) Measurements in a combustor operated on alternative liquid fuels. In 50th AIAA Aerospace Sciences Meeting including the new horizons forum and aerospace exposition, Nashville, TN, USA, AIAA Paper no. 2012-0524

Jiang L, Taylor RP, Agrawal AK (2012b) Emissions and temperature measurements in glycerol flames. In the 2012 Spring technical meeting of the central states section of the combustion institute, Dayton, OH, USA, Paper no. 030AF-0119

Keane RD, Adrian RJ (1992) Theory of cross-correlation analysis of PIV images. Appl Sci Res 49:191–215

Kourmatzis A, Masri AR (2014) The influence of gas phase velocity fluctuations on primary atomization and droplet deformation. Exp Fluids 55:1659. doi:10.1007/s00348-013-1659-3

Lefebvre AH (1980) Airblast atomization. Prog Energy Combust Sci 6(3):233–261

Lefebvre AH (1989) Atomization and sprays. Hemisphere Pub Corp, New York

Lefebvre AH (1992) Twin-fluid atomization: factors influencing mean drop size. At Sprays 2(2):101–119

Lin KC, Carter C, Fezzaa K, Liu Z, Wand J (2009) Studies of pure- and aerated-liquid jets using the X-ray phase contrast imaging. 11th I class international conference on liquid atomization and spray systems, Vail, CO, USA

Lin KC, Rajnicek C, McCall J, Carter C, Fezzaa K (2011) Investigation of pure- and aerated-liquid jets using X-ray phase contrast imaging technique. Nucl Instrum Methods Phys Res Sect A 649(1):194–196

Lin KC, Carter C, Smith S, Kastengren A (2014) Exploration of near-field plume properties for aerated-liquid jets using X-ray radiography. AIAA Paper no. 2014-1183

Linne M, Sedarsky D, Meyer T, Gord J, Carter C (2010) Ballistic imaging in the near-field of an effervescent spray. Exp Fluids 49:911–923

Mirsepassi A, Rankin DD (2014) Particle image velocimetry in viscoelastic fluids and particle interaction effects. Exp Fluids 55:1641. doi:10.1007/s00348-013-1641-0

Ohnesorge W (1936) Formation of drops by nozzles and the breakup of liquid jests. Z Angew Math Mech 16:355–358

Panchasara HV, Simmons BM, Agrawal AK (2009a) Combustion performance of biodiesel and diesel–vegetable oil blends in a simulated gas turbine burner. J Eng Gas Turb Power 131(3):1–11

Panchasara HV, Sequera D, Schreiber W, Agrawal AK (2009b) Combustion performance of a novel injector using flow-blurring for efficient fuel atomization. J Propul Power 25(4):984–987

Quispe CA, Coronado CR, Carvalho JA Jr (2013) Glycerol: production, consumption, prices, characterization and new trends in combustion. Renew Sust Energe Rev 27:475–493

Raghavan V, Rajesh S, Parag S, Avinash V (2009) Investigation of combustion characteristics of biodiesel and its blends. Combust Sci Technol 181(6):877–891

Rayleigh L (1883) Investigation of the character of the equilibrium of an incompressible heavy fluid of variable density. Proc Lond Math Soc 14:170–177. doi:10.1112/plms/s1-14.1.170

Rottenkolber G, Gindele J, Raposo J, Dullenkopf K, Hentschel W, Wittig S, Spicher U, Merzkirch W (2002) Spray analysis of a gasoline direct injector by means of two-phase PIV. Exp Fluids 32:710–721

Sarkar UK, Ramamurthi K (2007) Flow visualization of sprays formed by bubbly, slug, and annular flows in an effervescent atomizer. J Flow Vis Image Process 14:397–408

Sedarsky D, Idlahcen S, Roze C, Blaisot JB (2013) Velocity measurements in the near field of a diesel fuel injector by ultrafast imagery. Exp Fluids 54:1451. doi:10.1007/s00348-012-1451-9

Shepard TG (2011) Bubble size effect on effervescent atomization. Dissertation, The University of Minnesota

Simmons BM (2011) Atomization and combustion of liquid biofuels. Dissertation, The University of Alabama

Simmons BM, Agrawal AK (2010) Spray characteristics of a flow blurring atomizer. At Sprays 20(9):821–825

Simmons BM, Agrawal AK (2012) Flow blurring atomization for low-emission combustion of liquid biofuels. Combust Sci Technol 184(5):660–675

Simmons BM, Panchasara HV, Agrawal AK (2009) A comparison of air-blast and flow blurring injectors using phase Doppler particle analyzer techniques. In ASME Turbo Expo 2009: power for Land, Sea and Air, Orlando, FL, USA, ASME Paper no. GT2009-60239

Sovani SD, Sojka PE, Lefebvre AH (2001) Effervescent atomization. Prog Energ Combust 27(4):483–521

Steinmetz SA, Herrington JS, Winterrowd CK, Roberts WL, Wendt JOL, Linak WP (2013) Crude glycerol combustion: particulate, acrolein, and other volatile organic emissions. Proc Combust Inst 34(2):2749–2757

Szybist JP, Song J, Alam M, Boehman AL (2007) Biodiesel combustion, emissions and emission control. Fuel Process Technol 88(7):679–691

Taylor SGI (1950) The instability of liquid surfaces when accelerated in a direction perpendicular to their planes. Proc R Soc Lond B Biol Sci 201(1065):192–196. doi:10.1098/rspa.1950.0052

Tropea C (2011) Optical particle characterization in flows. Annu Rev Fluid Mech 43:399–426

Wang X, Huang Z, Kuti OA, Zhang W, Nishida K (2011) An experimental investigation on spray, ignition and combustion characteristics of biodiesels. Proc Combust Inst 33(2):2071–2077

Weber C (1931) Disintegration of liquid jets. Z Angew Math Mech 11:136–159